

Large enhancement of thermoelectric effects in a double quantum dot system due to interference and Coulomb correlation phenomena

Piotr Trocha^{1,*} and Józef Barnaś^{1,2,†}

¹*Faculty of Physics, Adam Mickiewicz University, 61-614 Poznań, Poland*

²*Institute of Molecular Physics, Polish Academy of Sciences, 60-179 Poznań, Poland*

(Dated: September 25, 2018)

Thermoelectric effects in a double quantum dot system coupled to external magnetic/nonmagnetic leads are investigated theoretically. The basic thermoelectric transport characteristics, like thermopower, electronic contribution to heat conductance, and the corresponding figure of merit, have been calculated in terms of the linear response theory and Green function formalism in the Hartree-Fock approximation for Coulomb interactions. An enhancement of the thermal efficiency (figure of merit ZT) due to Coulomb blockade has been found. The magnitude of ZT is further considerably enhanced by quantum interference effects. Both the Coulomb correlations and interference effects lead to strong violation of the Wiedemann-Franz law. The influence of spin-dependent transport and spin bias on the thermoelectric effects (especially on Seebeck and spin Seebeck effects) is also analyzed.

PACS numbers: 73.23.-b, 73.63.Kv, 73.50.Lw, 84.60.Bk, 85.80.Fi

I. INTRODUCTION

Energy conversion based on thermoelectric properties of solid-state materials has been attracting recently much attention, especially in the case of nanoscale systems. Although thermoelectric phenomena have been known for long time, their efficiency in bulk materials was relatively low, and therefore systems of high thermoelectric efficiency are greatly desired. The efficiency is usually measured by the dimensionless thermoelectric figure of merit ZT , $ZT = \sigma S^2 T / \kappa$. Here, T stands for the temperature, σ is the charge conductivity, S is the Seebeck coefficient (thermopower), and κ is the thermal conductivity which generally includes the phonon and electronic contributions. From this formula it is clear that to enhance the efficiency of a thermoelectric device one has to somehow enlarge the thermopower S and electric conductivity σ , and reduce the thermal conductivity κ . However, this task is difficult to be realized in conventional materials which obey the Wiedemann-Franz law.¹ Moreover, the Seebeck coefficient becomes decreased as the charge conductance increases due to the Mott relation.² Typically observed values of ZT are smaller than one, $ZT \lesssim 1$, and this is why thermoelectric materials have not been widely used in commercial applications.

It has turned out recently, that this drawback of bulk materials can be overcome in nanoscale systems. Hick *et al.*³ have predicted an increase of the figure of merit as the dimension of the system is reduced. Now, it is well known that the thermoelectric properties of nanoscale systems are strongly affected by quantum confinement (level quantization) and Coulomb blockade effects.^{4–10} These effects can lead to violation of the Wiedemann-Franz law and failure of the Mott relation.^{11,12} Moreover, the thermal conductance of low dimensional systems is rather small, which allows to reach rather high values of ZT .¹³ Owing to these properties of nanoscale struc-

tures, which are promising from the application point of view, interest in thermoelectric phenomena revived in recent years. Accordingly, thermoelectric properties of quantum dots (QDs), quantum wires, molecules and silicon nanojunctions have been investigated both experimentally^{14–18} and theoretically.^{19–28} Oscillations of the thermopower^{4,5} and thermal conductance^{9,11} with external gate voltage have been reported in thermoelectric transport through Coulomb islands. Moreover, it has been shown that spin correlations can strongly influence the thermoelectric effects in the Kondo regime.^{29–37} Recently, an increase of the thermal efficiency has been reported in a multilevel QD for temperatures much smaller than the intradot charging energy.^{38–40} Furthermore, the influence of ferromagnetic leads (spin polarized current) on thermoelectric transport properties in a single-level QD has been also investigated in different coupling regimes.^{20,21} In turn, Hatami *et al.* have analyzed the Peltier and Seebeck phenomena in magnetic multilayered structures and shown that the thermoelectric effects significantly depend on the relative alignment of magnetizations in neighboring magnetic layers.⁴¹ For a more comprehensive description of various thermoelectric transport properties in nanostructures we refer to recent review articles.^{42–44}

However, the thermoelectric phenomena in multiple quantum dot systems are rather unexplored.^{45–48} Especially, double quantum dot systems may exhibit some new thermoelectric phenomena as they reveal a variety of different interference effects, including Fano and Dicke resonances^{49,50} or Aharonov-Bohm oscillations.⁵¹ The Fano effect appears due to quantum interference of waves resonantly transmitted through a discrete level and those transmitted nonresonantly through continuum of states. The effect was first observed as an asymmetric line shape of atomic emission spectra, but it also appears in electronic transport through QD systems. In the case of double QDs, the Fano effect originates from

the quantum interference of electron waves transmitted coherently through the weakly coupled state to the leads and those transmitted through the state which is strongly coupled to the external electrodes.^{49,52} Very recently Liu *et al.* have investigated thermoelectric effects in parallel double QDs attached to two metallic leads, and with a magnetic flux threading the quantum dot device.⁵³ They arrived to the conclusion that the figure of merit ZT can be enhanced in the vicinity of the Fano resonance. Similar conclusion also follows from a recent paper⁵⁴, where the influence of electron interference in a two-level system on the maximum thermoelectric power is analyzed.

Recently, the spin voltage generated by a temperature gradient has been observed experimentally in a metallic magnet.⁵⁵ This novel phenomenon, called spin Seebeck effect, offers a new way for generation of a pure spin current without accompanying charge current. The discovery of spin Seebeck effect has stimulated both experimental and theoretical interest in the so-called spin caloritronics. Although the spin caloritronics is as old as spin electronics⁵⁶, it has been poorly investigated and has remained dormant for many years – except of a few experimental works on the thermoelectric properties of magnetic multilayers in the current-in-plane geometry.⁵⁷ More recently spin-dependent heat and charge transport in magnetic multilayers was studied experimentally in the perpendicular-to-plane geometry.^{58,59} As concerns spin thermoelectric effects in quantum dot systems, these are rather poorly explored although interest in them has been growing recently.^{21,60–62}

In this paper we consider thermoelectric effects in the system consisting of parallel coupled quantum dots embedded between metallic (normal or ferromagnetic) leads. In contrast to Ref.[53], we include the Coulomb correlations. The latter are long range interactions and therefore can not be excluded in realistic systems. Moreover, one can expect a significant enhancement of the thermal efficiency in the Coulomb blockade regime. The basic thermoelectric characteristics are derived using nonequilibrium Green function method. The Coulomb correlations are taken in the Hartree-Fock approximation and thus the formalism is relevant for temperatures higher than the specific temperature associated with the Kondo effect (Kondo temperature). Additionally, we investigate the spin Seebeck effect, too. In Section II we present the model of a double quantum dot system attached to ferromagnetic/nonmagnetic leads and describe basic thermoelectric phenomena to be analyzed. In Sec. III we present the corresponding numerical results. Finally, Sec. IV includes summary and general conclusions.

II. THEORETICAL DESCRIPTION

A. Model

We consider two single-level quantum dots which are attached to normal/magnetic metallic leads. Since the inter-dot Coulomb interaction is small in comparison to the intra-dot one, the former will be omitted in the following. The system is then described by Hamiltonian of the form

$$\begin{aligned} \hat{H} = & \sum_{\mathbf{k}\beta\sigma} \varepsilon_{\mathbf{k}\beta\sigma} c_{\mathbf{k}\beta\sigma}^\dagger c_{\mathbf{k}\beta\sigma} + \sum_{\mathbf{k}\beta} \sum_{i\sigma} (V_{i\mathbf{k}\sigma}^\beta c_{\mathbf{k}\beta\sigma}^\dagger d_{i\sigma} + \text{h.c.}) \\ & + \sum_{i\sigma} \varepsilon_{i\sigma} d_{i\sigma}^\dagger d_{i\sigma} - t \sum_{\sigma} (d_{1\sigma}^\dagger d_{2\sigma} + \text{h.c.}) + \sum_i U_i n_{i\sigma} n_{i\bar{\sigma}} \end{aligned} \quad (1)$$

where the first term describes the left ($\beta = L$) and right ($\beta = R$) leads in the non-interacting quasi-particle approximation. Here, $c_{\mathbf{k}\beta\sigma}^\dagger$ ($c_{\mathbf{k}\beta\sigma}$) is the creation (annihilation) operator of an electron with the wave vector \mathbf{k} and spin σ in the electrode β , whereas $\varepsilon_{\mathbf{k}\beta\sigma}$ denotes the corresponding single-particle energy. The second term of Hamiltonian (1) describes spin conserving electron tunneling between the leads and i th dot ($i = 1, 2$), with $V_{i\mathbf{k}\sigma}^\beta$ being the relevant matrix elements. The last three terms describe two quantum dots, where $\varepsilon_{i\sigma}$ denotes the discrete energy level of the i -th dot, $n_{i\sigma} = d_{i\sigma}^\dagger d_{i\sigma}$ is the corresponding particle number operator, t is the inter-dot hopping parameter (assumed real and independent of the electron spin orientation), whereas U_i is the Coulomb energy corresponding to double occupation of the i -th dot ($i = 1, 2$).

The dot-leads coupling is described usually by the width functions $\Gamma_{ij\sigma}^\beta = 2\pi\rho_\beta^\sigma V_i^\beta V_j^{\beta*}$, where ρ_β^σ is the density of states in the lead β for spin σ . $\Gamma_{ij\sigma}^\beta$ describes the spin-dependent hybridization of the dots' levels ($i, j = 1, 2$) and states of the β th lead. For the sake of simplicity we assume that the couplings are constant within the electron band; $\Gamma_{ij\sigma}^\beta(\varepsilon) = \Gamma_{ij\sigma}^\beta = \text{const}$ for $\varepsilon \in \langle -D, D \rangle$, and $\Gamma_{ij\sigma}^\beta(\varepsilon) = 0$ otherwise, where $2D$ denotes the electron band width.

The coupling parameters can be written in a matrix form as

$$\mathbf{\Gamma}_\sigma^\beta = \begin{pmatrix} \Gamma_{11\sigma}^\beta & q_\beta \sqrt{\Gamma_{11\sigma}^\beta \Gamma_{22\sigma}^\beta} \\ q_\beta \sqrt{\Gamma_{11\sigma}^\beta \Gamma_{22\sigma}^\beta} & \Gamma_{22\sigma}^\beta \end{pmatrix}, \quad (2)$$

for $\beta = L, R$. To take into account various interference effects leading to suppression of the nondiagonal terms, we have introduced the parameters q_L and q_R . These parameters are generally complex, and $0 \leq |q_\beta| \leq 1$. The spin-dependent coupling strengths can be then written as; $\Gamma_{11\sigma}^L = \Gamma_L(1 \pm p_L)$, $\Gamma_{12\sigma}^L = \Gamma_{21\sigma}^L = q_L \Gamma_L \sqrt{\alpha}(1 \pm p_L)$, $\Gamma_{22\sigma}^L = \alpha \Gamma_L(1 \pm p_L)$, $\Gamma_{11\sigma}^R = \alpha \Gamma_R(1 \pm \delta p_R)$, $\Gamma_{12\sigma}^R = \Gamma_{21\sigma}^R = q_R \Gamma_R \sqrt{\alpha}(1 \pm \delta p_R)$, and $\Gamma_{22\sigma}^R = \Gamma_R(1 \pm \delta p_R)$ with

$\delta = 1$ for parallel magnetic configuration and $\delta = -1$ for the antiparallel one. The upper sign refers here to $\sigma = \uparrow$, while the lower sign refers to $\sigma = \downarrow$. Apart from this, p_β ($\beta = L, R$) is the polarization factor of the β -th lead, Γ_L and Γ_R are the coupling constants, and α takes into account difference in the coupling of a given electrode to the two dots. For $\alpha = 0$ the system becomes reduced to two QDs connected in series.

B. Thermoelectric phenomena

Consider first the situation when chemical potentials of the leads are independent of spin orientation (no spin accumulation). The charge current J , spin current J^s , and heat current of electronic origin J^Q , flowing from the left lead to the right one, can be determined from the following formula:

$$\begin{pmatrix} J \\ J^s \\ J^Q \end{pmatrix} = \frac{1}{h} \sum_{\sigma} \int d\varepsilon \begin{pmatrix} e \\ \hat{\sigma}\hbar/2 \\ \varepsilon - \mu_L \end{pmatrix} [f_L(\varepsilon) - f_R(\varepsilon)] T_{\sigma}(\varepsilon), \quad (3)$$

where $f_{\beta}(\varepsilon) = \{\exp[(\varepsilon - \mu_{\beta})/k_B T_{\beta}] + 1\}^{-1}$ is the Fermi-Dirac distribution function for the lead β with μ_{β} and T_{β} denoting the corresponding chemical potential and temperature, and k_B standing for the Boltzmann constant. Furthermore, $T_{\sigma}(\varepsilon)$ is the sum of transmission coefficients through the two conducting channels associated with two dots for carriers with spin σ ($\sigma = \uparrow, \downarrow$), and $\hat{\sigma} = 1$ for $\sigma = \uparrow$ and $\hat{\sigma} = -1$ for $\sigma = \downarrow$. $T_{\sigma}(\varepsilon)$ can be expressed by the Fourier transforms of retarded (\mathbf{G}_{σ}^r) and advanced (\mathbf{G}_{σ}^a) Green functions of the dots and by the coupling matrices $\mathbf{\Gamma}_{\sigma}^{\beta}$ ($\beta = L, R$); $T_{\sigma}(\varepsilon) = \text{Tr}[\mathbf{G}_{\sigma}^a \mathbf{\Gamma}_{\sigma}^R \mathbf{G}_{\sigma}^r \mathbf{\Gamma}_{\sigma}^L]$. The Green functions have been calculated by the equation of motion technique in the Hartree-Fock approximation for the Coulomb term.⁴⁹

In the linear response regime, Eq.(3) can be transformed to the following formulas for charge, spin, and heat currents:

$$J = \sum_{\sigma} J_{\sigma} \equiv e \sum_{\sigma} L_{0\sigma} \delta\mu + \frac{e}{T} \sum_{\sigma} L_{1\sigma} \delta T, \quad (4)$$

$$J^s = \sum_{\sigma} J_{\sigma}^s = \frac{\hbar}{2} \sum_{\sigma} \hat{\sigma} L_{0\sigma} \delta\mu + \frac{\hbar}{2T} \sum_{\sigma} \hat{\sigma} L_{1\sigma} \delta T, \quad (5)$$

$$J^Q = \sum_{\sigma} J_{\sigma}^Q \equiv \sum_{\sigma} L_{1\sigma} \delta\mu + \frac{1}{T} \sum_{\sigma} L_{2\sigma} \delta T, \quad (6)$$

where δT is the difference in temperatures of the leads, and $\delta\mu = e\delta V$ with δV being the voltage drop between the two electrodes. We remind, that according to our assumption, the chemical potential and temperature of the left electrode are $\mu + \delta\mu$ and $T + \delta T$, respectively, whereas of the right electrode are μ and T . Note, that in the linear response regime both $\delta\mu$ and δT tend to

zero. In Eqs. (4) to (6) $L_{n\sigma}$ ($n = 0, 1, 2; \sigma = \uparrow, \downarrow$) are the integrals of the form

$$L_{n\sigma} = -\frac{1}{h} \int d\varepsilon (\varepsilon - \mu)^n \frac{\partial f}{\partial \varepsilon} T_{\sigma}(\varepsilon). \quad (7)$$

The thermopower S is defined as the ratio of the voltage drop δV generated by the temperature difference δT , $S = \delta V / \delta T$, taken in the absence of charge current, $J = 0$. Thus, taking into account Eq.(4) and Eq.(6), one obtains the following formula for the Seebeck coefficient:

$$S \equiv \left[\frac{\delta V}{\delta T} \right]_{J=0} = -\frac{1}{eT} \frac{\sum_{\sigma} L_{1\sigma}}{\sum_{\sigma} L_{0\sigma}}. \quad (8)$$

Similarly, the charge and spin conductances, G and G^s , can be expressed in terms of the integrals (7) as⁶³

$$G = e^2 \sum_{\sigma} L_{0\sigma}, \quad (9)$$

$$G^s = \frac{e\hbar}{2} \sum_{\sigma} \hat{\sigma} L_{0\sigma}, \quad (10)$$

while the thermal conductance can be written as

$$\kappa = \frac{1}{T} \left(\sum_{\sigma} L_{2\sigma} - \frac{[\sum_{\sigma} L_{1\sigma}]^2}{\sum_{\sigma} L_{0\sigma}} \right). \quad (11)$$

Note that the thermal conductance is determined on the condition of vanishing charge current. Thus, to determine the basic thermoelectric parameters we need to find all the relevant integrals, $L_{0\sigma}$, $L_{1\sigma}$, and $L_{2\sigma}$.

Consider now a more general situation, when spin accumulation in the external leads becomes relevant, eg. due to long spin relaxation time or when an external spin dependent bias is applied to the system. In such a case we have to take into account spin splitting of the chemical potential in the leads. In a general case, temperature may also be different in different spin channels. However, we neglect this assuming T independent of σ . This may be justified as the energy relaxation time is much shorter than the spin relaxation one. Equations (3) take now the form

$$\begin{pmatrix} J \\ J^s \\ J^Q \end{pmatrix} = \frac{1}{h} \sum_{\sigma} \int d\varepsilon \begin{pmatrix} e \\ \hat{\sigma}\hbar/2 \\ \varepsilon - \mu_L \end{pmatrix} [f_{L\sigma}(\varepsilon) - f_{R\sigma}(\varepsilon)] T_{\sigma}(\varepsilon), \quad (12)$$

where the spin dependence of the Fermi distribution function is now indicated explicitly. Thus, charge, spin and heat currents can still be expressed in the form of Eqs (4) to (6), but with $\delta\mu$ being explicitly dependent on σ , $\delta\mu \rightarrow \delta\mu_{\sigma}$, and $L_{n\sigma}$ including now derivative of spin dependent Fermi distribution function.

Since the bias is now spin dependent, the difference in chemical potentials, $\delta\mu_{\sigma}$, in the spin channel σ can be written as

$$\delta\mu_{\sigma} = e\delta V_{\sigma} = e(\delta V + \hat{\sigma}\delta V^s), \quad (13)$$

where δV is the voltage bias and δV^s is the spin bias²¹. Of course, $\delta V^s = 0$ in the absence of spin accumulation.

Charge and spin currents can be written as $J = G\delta V + (2e/\hbar)G^s\delta V^s$, where G and G^s are the linear charge and spin conductances defined above (see Eqs (9) and (10)). In turn, the spin current can be written as $J^s = G^s\delta V + (\hbar/2e)G\delta V^s$.

The thermopower can be now calculated on the condition of vanishing simultaneously both spin current and charge current, or equivalently on the condition of vanishing charge current in each spin channel. As a result, one can define spin dependent thermopower as

$$S_\sigma = \frac{\delta V_\sigma}{\delta T} = -\frac{L_{1\sigma}}{eTL_{0\sigma}}. \quad (14)$$

Equivalently, one can define spin thermopower S^s

$$S^s = \frac{\delta V^s}{\delta T} = \frac{1}{2}(S_\uparrow - S_\downarrow) = -\frac{1}{2eT} \left(\frac{L_{1\uparrow}}{L_{0\uparrow}} - \frac{L_{1\downarrow}}{L_{0\downarrow}} \right) \quad (15)$$

in addition to the usual thermopower

$$S = \frac{\delta V}{\delta T} = \frac{1}{2}(S_\uparrow + S_\downarrow) = -\frac{1}{2eT} \left(\frac{L_{1\uparrow}}{L_{0\uparrow}} + \frac{L_{1\downarrow}}{L_{0\downarrow}} \right). \quad (16)$$

In turn, the heat conductance is then given by

$$\kappa = \sum_\sigma \kappa_\sigma \equiv \frac{1}{T} \sum_\sigma \left(L_{2\sigma} - \frac{L_{1\sigma}^2}{L_{0\sigma}} \right). \quad (17)$$

In the following we use the above formulas to calculate numerically the relevant thermoelectric coefficients.

III. NUMERICAL RESULTS

For numerical calculations we assume spin degeneracy and equal dot levels, $\varepsilon_{i\sigma} = \varepsilon_0$ (for $i = 1, 2$ and $\sigma = \uparrow, \downarrow$). We also assume similar magnetic electrodes, $p_L = p_R \equiv p$, and symmetrical couplings, $\Gamma_L = \Gamma_R \equiv \Gamma$. Typical experimental values of the dot-lead coupling may vary from a few microelectronvolts to a few milielectronvolts.⁶⁴ In the following it is convenient to relate energy quantities to the dot-lead coupling. To have unique energy units, we write the parameter Γ as $\Gamma = \gamma\Gamma_0$, where Γ_0 is constant and will be treated as the energy unit (the energy quantities will be related to Γ_0). In turn, γ is a dimensionless parameter that describes strength of the dot-lead coupling in terms of Γ_0 .

The case of nonmagnetic leads is treated as a special case corresponding to $p = 0$. The parameters q_L and q_R are assumed to be real and equal, $q_L = q_R = q$. In turn, for the parameter α we assume $\alpha = 0.15$, which indicates that there is a relatively large difference in the coupling of a given electrode to the two dots. This parameter, however, can be tuned by external gate voltages. For the sake of simplicity we also assume the same Coulomb parameters for the two dots, $U_1 = U_2 = U$.

In a general case, the electrochemical potentials of the leads may be spin dependent. In other words, in addition to the usual voltage bias one may also consider spin bias. The latter may appear when spin relaxation in the leads is slow so a spin accumulation may appear due to the spin bottle-neck effect (or simply when a spin bias is applied intentionally). This leads to a number of spin thermoelectric effects. We start from the simpler case when the spin relaxation in the leads is sufficiently fast to neglect spin accumulation, so the leads' electrochemical potentials are independent of the electron spin orientation.

A. Absence of spin bias

Since the thermoelectric effects considered in the manuscript depend on spin polarization of the leads, we consider first the situation with nonmagnetic electrodes, and then proceed to magnetic leads.

1. Nonmagnetic leads: $p = 0$

The effects considered in this paper depend significantly on the ratio of thermal energy and coupling strength of the dots to electrodes. Let us consider first the low temperature regime, $k_B T \ll \Gamma$, or in our notation, $k_B T/\Gamma_0 \ll \gamma$. We have calculated the basic thermoelectric characteristics, like thermopower S , heat conductance κ , charge conductance G , and figure of merit ZT . Although we consider the regime $k_B T \ll \Gamma$, the temperature assumed here is higher than the corresponding Kondo temperature, so we do not take into account the Kondo correlations. In this transport regime one finds generally $ZT \ll 1$.¹² However, this can be changed by quantum interference effects.

Let us begin with the case of vanishing Coulomb interaction, $U = 0$. In Fig.1 the thermoelectric quantities are plotted as a function of the dots' energy levels ε_0 for $t/\Gamma_0 = 0.8$ and for indicated values of the parameter q . The latter parameter effectively describes strength of the indirect (via the leads) coupling of the dots. Such a coupling contributes (like direct inter-dot hopping term) to the formation of bonding and antibonding states. As a result, a broad peak corresponding to the bonding state and a narrow one corresponding to the antibonding state emerge in the density of states.⁴⁹ For q close to 1, the conductance peak associated with the antibonding state reveals the antiresonance character with a characteristic Fano line shape, whereas the conductance peak associated with the bonding state is relatively broad and roughly Lorentzian. For smaller (but nonzero) values of the parameter q , the antiresonance is suppressed and one observes two peaks of different widths. Finally, for $q = 0$ two peaks of equal widths emerge in the linear conductance. Similar line shape and q dependence is observed in the electronic contribution to the heat conductance,

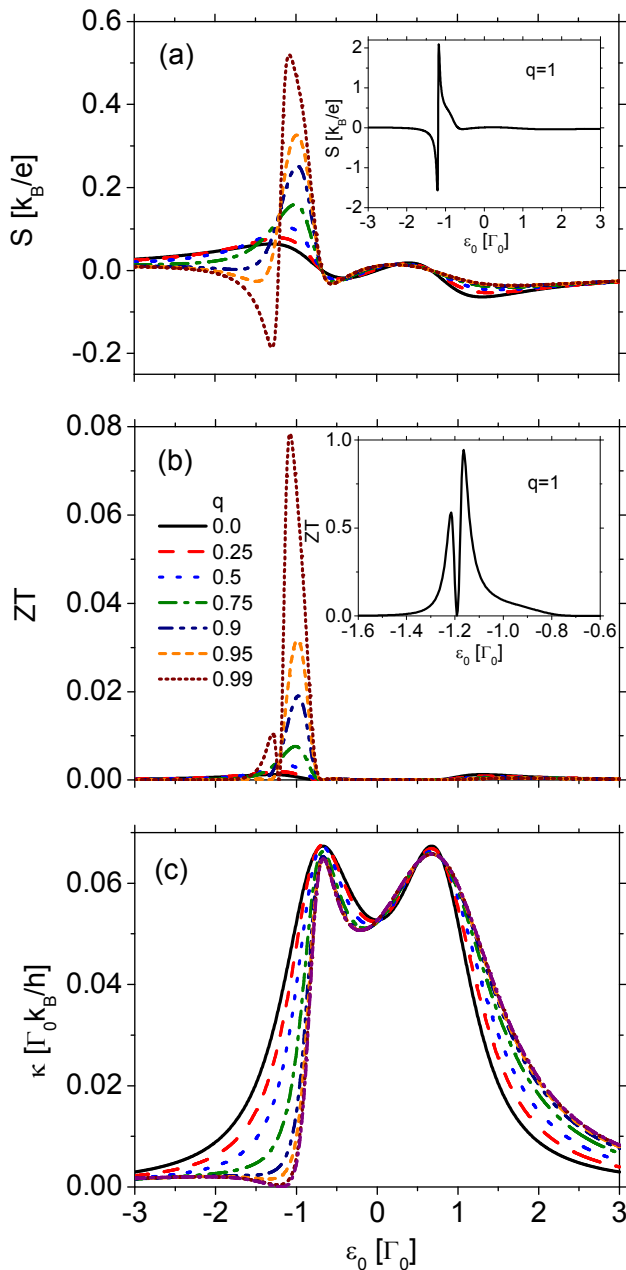


FIG. 1: (color online) Thermoelectric coefficients: (a) thermopower, (b) the figure of merit, (c) thermal conductance, calculated as a function of the dots' levels energy for indicated values of the parameter q . The other parameters are $k_B T/\Gamma_0 = 0.01$, $t/\Gamma_0 = 0.8$, $\alpha = 0.15$, $U = 0$, $\gamma = 1$, and $p = 0$. The insets in (a) and (b) show respectively the thermopower S and figure of merit ZT for $q = 1$.

as shown in Fig.1(c). Positions of the peaks in thermal conductance correspond well to those in the electric conductance, similarly as in the case of a single dot.²¹

The thermopower S , shown in Fig.1(a), changes sign when ε_0 corresponds to one of the relevant resonances. This is a consequence of the compensation of charge current due to electrons by that due to holes. As a re-

sult, there is no net charge current and no voltage drop, and consequently the thermopower vanishes. When the energy level is located below the resonance, the thermopower is negative because the majority carriers are holes. In turn, when the energy level is above the resonance the main carriers are electrons and thus the thermopower is positive. Note that S in Fig.1(a) is measured in the units of k_B/e , with e denoting electron charge ($e < 0$). However, when q is close to 1, one finds two more points where the thermopower changes sign. One of them is situated near the Fano resonance, where the conductance vanishes due to destructive interference, whereas the other one is located in the valley between the two resonances. For other values of q only the point in the valley between the resonances is present, as no complete destructive interference occurs for smaller q . The largest increase of the thermopower appears in the vicinity of the antibonding resonance and for $q = 1$. This shows that the quantum interference has a huge impact on the thermoelectric phenomena. This is also clearly visible in the figure of merit ZT , shown in Fig.1(b), which is considerably enhanced in the vicinity of the Fano antiresonance, where ZT is close to 1. Outside this region ZT is significantly suppressed, even near the bonding energy level. When q decreases, the figure of merit ZT (which reaches almost unity for $q = 1$ near the Fano resonance) diminishes as well. Thus, the interference effects play a crucial role in thermoelectric efficiency of DQD systems considered here. However, in this coupling regime ($k_B T \ll \Gamma$) the Wiedemann-Franz law is not violated much as the Lorenz number (not shown) remains close to unity.

Consider now the impact of Coulomb repulsion on the thermoelectric properties in the presence of Fano resonance, see Fig.2. First, the Coulomb interaction leads to splitting of the double-peak structure (present for $U = 0$) in both the charge and thermal conductance, and characteristic Coulomb gaps occur⁴⁹ (see Fig.2(c) for the thermal conductance). This doubling of the resonances also leads to a richer structure of the thermopower. For a finite U the thermopower changes sign ten times, see Fig.2(a). Four points of zero S are associated with the four resonances located roughly at $\pm t$ and $\pm t - U$. Next two such points are located near the Fano peak and its Coulomb counterpart, where the conductance disappears (so does the thermopower), whereas two other points are situated in the valleys between the narrow and broad maxima of the conductance. In the latter case the thermopower vanishes due to weighted-symmetry in location of the bonding and antibonding states with respect to the Fermi level. The current due to electrons tunneling through the bonding state is compensated then by the current due to holes tunneling through the antibonding level. This is a 'local' bipolar effect. The thermopower disappears also in the symmetry point $\varepsilon = -U/2$, as it has been explained in Ref.[21]. However, there is one more point where the thermopower changes sign, namely this happens at the energy where a small maximum appears in the Coulomb gap (this feature is due to a rem-

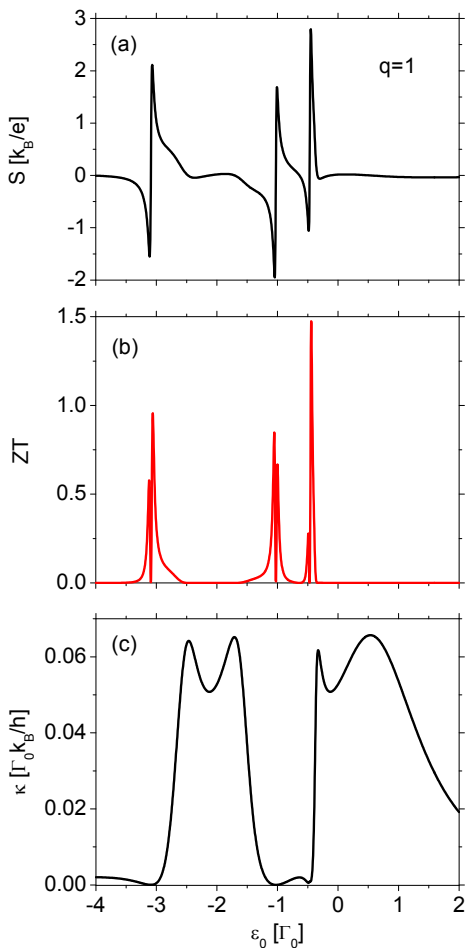


FIG. 2: (color online) Thermopower S (a), figure of merit ZT (b), and the thermal conductance (c), calculated as a function of the dots' levels energy for $U/\Gamma_0 = 2$ and $q = 1$. The other parameters as in Fig.1.

nant of the conductance maximum corresponding to the antibonding state). Correspondingly, more peaks occur in the figure of merit, see Fig.2(b). From Figs 1 and 2 also follows that the Coulomb interactions can increase the magnitude of ZT , which now exceeds 1. However, ZT is considerably enhanced only near the Fano antiresonances (as in the case of $U = 0$) and also in the middle of the Coulomb gap. The latter is due to a global bipolar effect.

Above we have analyzed the range of $k_B T/\Gamma \ll 1$. The thermal efficiency, however, strongly depends on the ratio of thermal energy and coupling strength, and for $k_B T/\Gamma > 1$ one might expect an increase of the thermal efficiency.¹² On the other side, however, higher temperature suppresses the interference effects responsible for the Fano antiresonance. In Fig. 3 we show the temperature dependence of the thermoelectric coefficients for the level position near the antibonding state and vanishing Coulomb interactions. The results clearly show that the thermoelectric effects are optimized for $k_B T/\Gamma \approx 10$, or equivalently $k_B T/\Gamma_0 \approx 10\gamma$. To show this more explic-

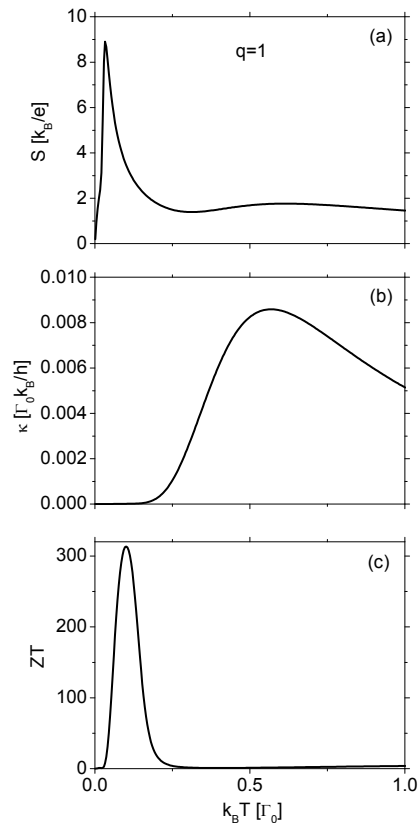


FIG. 3: (color online) Thermoelectric coefficients: (a) thermopower, (b) thermal conductance, (c) figure of merit, calculated as a function of temperature for the position of the dots' levels in the vicinity of the Fano resonance, $\varepsilon_0/\Gamma_0 = -1.15$, and for $q = 1$, $U = 0$, and $\gamma = 0.01$. The other parameters as in Fig.1.

itly, in Fig. 4 we present the temperature and level position dependence of the thermoelectric coefficients. Figure 4(c) clearly shows that the largest enhancement of the thermoelectric efficiency occurs in the vicinity of the antibonding level. Moreover, as the temperature grows, a strong increase of the thermal conductance is observed in the valley between the two low-temperature maxima of the conductance, see Fig. 4(a). Such a peak is absent in the electric conductance and also does not appear in thermal conductance in the low temperature regime. When the temperature is relatively high, the Fermi-Dirac distribution around the Fermi level becomes smeared, and electrons of higher energies are involved in transport. As the energy of tunneling electrons does not influence the electric conductance, it plays a crucial role in the thermal conductance. As already mentioned above, in the symmetry point, $\varepsilon_0 = -U/2$, the charge current due to electrons is compensated by current due to holes. However, both electrons and holes flow in the same direction, so the energy carried by both types of carriers is not compensated, in contrast to the charge. As a result, an additional peak centered at $\varepsilon_0 = -U/2$ appears in the thermal conductance for a sufficiently high temperature.

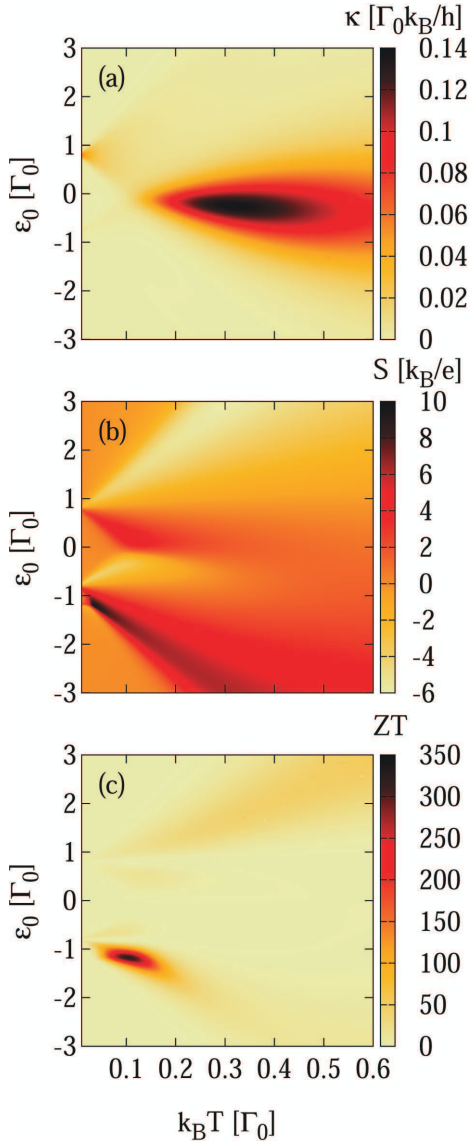


FIG. 4: Thermal conductance (a), thermopower (b), and the figure of merit (c), as a function of temperature and dots' levels energy for $q = 1$, $U = 0$, $\gamma = 0.01$, and the other parameters as in Fig.1.

The thermoelectric efficiency of the system under consideration can be further optimized by tuning asymmetry (parameter α) in the coupling of a given lead to the two dots. To show this, in Fig. 5 we present the α and level position dependence of the figure of merit for two distinct coupling regimes: $k_B T/\Gamma \ll 1$ (part (a)) and $k_B T/\Gamma > 1$ (part (b)). The thermoelectric efficiency in these two transport regimes is optimized for different ranges of the parameter α . In the low temperature regime ($k_B T/\Gamma \ll 1$), ZT is optimized for intermediate values of the asymmetry parameter, roughly for $\alpha \in \langle 0.3, 0.6 \rangle$. In turn for $k_B T/\Gamma > 1$, the figure of merit achieves the highest values for relatively high asymmetry, $\alpha \in \langle 0.1, 0.2 \rangle$. It is worth noting that in the former case the figure of merit

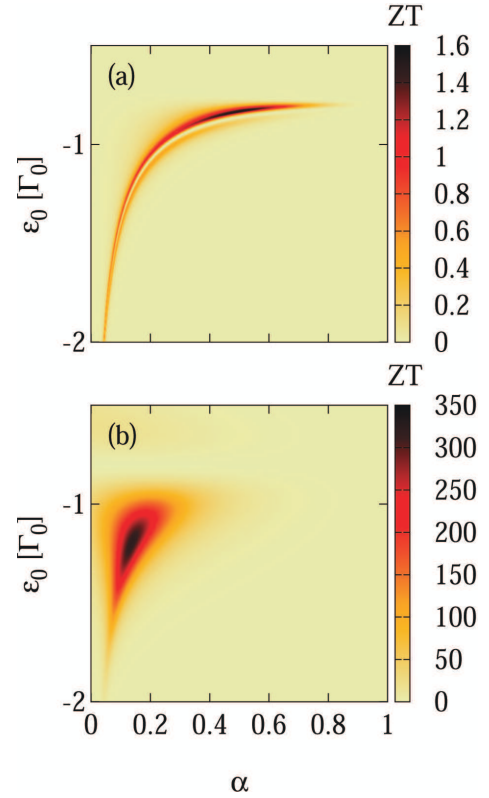


FIG. 5: Figure of merit as a function of the asymmetry parameter α and the dots' levels energy, calculated for $k_B T/\Gamma_0 = 0.01$ and $\gamma = 1$ (a), and $k_B T/\Gamma_0 = 0.1$ and $\gamma = 0.01$ (b). Apart from this, $q = 1$, $U = 0$, and the other parameters as in Fig.1.

ZT can exceed 1 for properly chosen asymmetry parameter α despite of relatively strong dot-lead coupling, while in the latter case ZT can reach extremely large values exceeding 300.

The strong dependence of ZT on the asymmetry parameter α , displayed in Fig. 5 (a), is due to the interference effects of electron waves passing through different paths in the system. More specifically, it originates from the α dependence of the position of the point where the electron conductance (as well as the thermal conductance) reaches almost zero due to the destructive quantum interference. At this point (and in its neighborhood) the thermoelectric effects are maximized, which is reflected by enhanced values of the figure of merit ZT in Fig. 5 (a). In turn, in the high temperature regime, Fig. 5 (b), the Fermi-Dirac distribution around the Fermi level becomes smeared and since the low and high energy electrons contribute differently to heat current, the thermal conductance peaks do not coincide now with those in the electric conductance (contrary to the low temperature regime where they do). Thus, behavior of the thermal conductance is now more complex. In the vicinity of the antibonding state, the thermal conductance is strongly suppressed achieving local minimum. This region of suppressed thermal conductance appears in the 'tail' of the

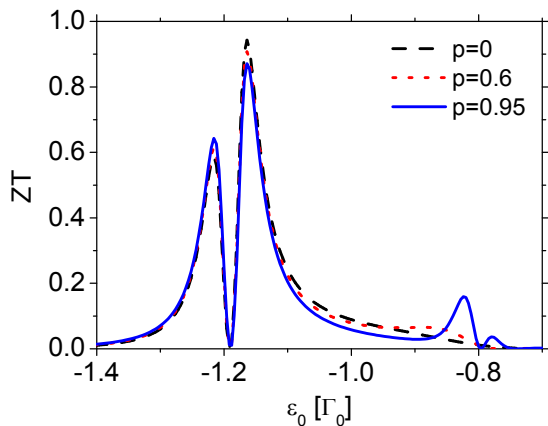


FIG. 6: (color online) Thermoelectric figure of merit ZT as a function of the dots' levels energy, calculated for indicated values of the leads' polarization p in the parallel magnetic configuration, and for $q = 1$, $U = 0$, $k_B T/\Gamma_0 = 0.01$ and $\gamma = 1$. The other parameters as in Fig.1.

electric conductance peak, where G is finite. Moreover, position of the minimum in thermal conductance depends on the asymmetry parameter α , while position of the peak in electric conductance is rather unchanged. This behavior leads to a large enhancement of ZT seen in Fig. 5(b) for $0.1 < \alpha < 0.2$. When α increases above 0.2, the intensity of the peak in electric conductance corresponding to the antibonding state becomes suppressed, and this leads to suppression of ZT for $\alpha > 0.2$. On the other hand the suppression of ZT for $\alpha < 0.1$ is associated with a strong dependence of the minimum position in the thermal conductance on the parameter α for $\alpha \in (0, 0.2)$.

2. Magnetic leads: $p > 0$

Now we consider the situation when both electrodes are ferromagnetic, with the corresponding spin polarization factor p . In the following only collinear, i.e. parallel and antiparallel, configurations will be analyzed.

In the coupling regime $k_B T/\Gamma \ll 1$, the Seebeck coefficient and figure of merit are only weakly dependent on the leads' polarization. As it has been mentioned above, ZT is enhanced only in the vicinity of the Fano resonance. For $U = 0$, one can notice the double narrow peak structure in ZT near the Fano resonance, see Fig.6, where ZT is shown for three different values of the spin polarization factor p (including for comparison also the case of $p = 0$). Between the peaks ZT reaches zero due to vanishing thermopower (as already explained above). However, an additional double peak feature in ZT appears for sufficiently large p , with the intensities (widths) increasing (decreasing) with increasing polarization. This feature is absent for small values of p (also for $p = 0$, see the inset to Fig.1(b)). The appearance of the second double peak structure can be accounted for as fol-

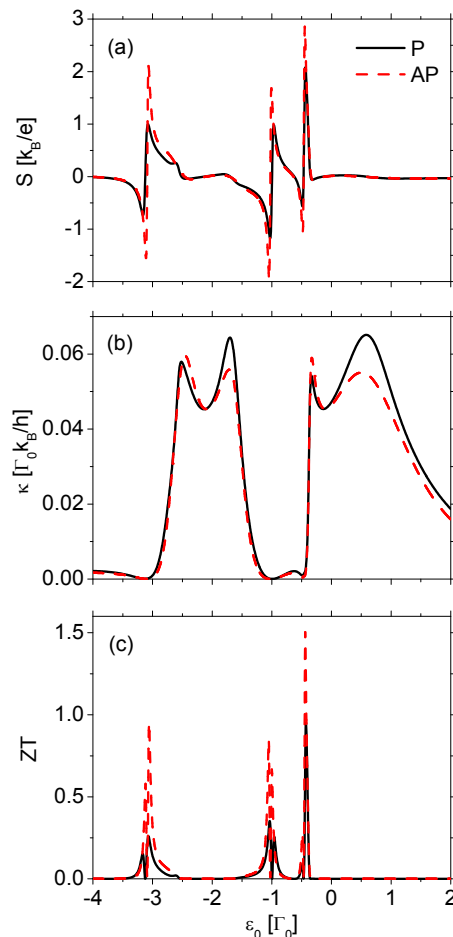


FIG. 7: (color online) Thermoelectric coefficients: (a) thermopower, (b) thermal conductance, (c) the figure of merit as a function of the dots' levels energy, calculated for parallel (P) and antiparallel (AP) magnetic configurations, and for $p = 0.4$, and $U/\Gamma_0 = 2$. The other parameters as in Fig.6.

lows: Since the coupling between the dots and external (magnetic) leads is spin-dependent for $p \neq 0$, the level widths of the bonding and antibonding states are spin dependent, too. This results in narrowing (broadening) of the conductance peak corresponding to the spin down (spin up) carriers. Consequently, the characteristic zero-conductance Fano point is achieved first in the spin-down channel when going towards larger negative values of ε_0 . This, in turn, results in well resolved sharp features in the Seebeck coefficient - one coming from spin-up contribution and another one (smaller) from the spin-down contribution. As a result, additional double-peak structure appears in the thermal conductivity (not shown) and also in the figure of merit, as in Fig.6. The role of finite U is similar to that described for $p = 0$.

The thermoelectric coefficients depend now on magnetic configuration of the system. In Fig.7 the thermopower, thermal conductance and figure of merit ZT are displayed for the parallel and antiparallel magnetic configurations and for a finite U . It is worth noting that

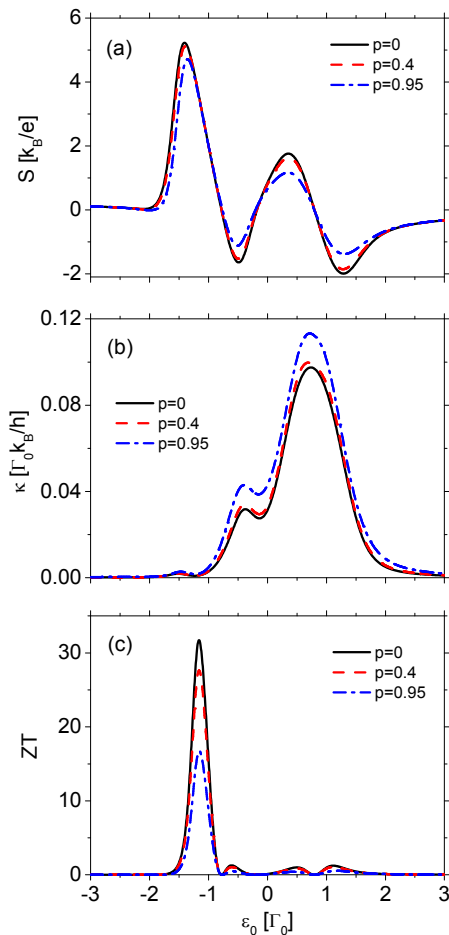


FIG. 8: (color online) Thermoelectric coefficients: (a) thermopower, (b) thermal conductance, (c) the figure of merit as a function of the dots' levels energy, calculated for indicated values of the leads' polarization p in the parallel magnetic configuration, and for $U/\Gamma_0 = 0$, $q = 1$, $k_B T/\Gamma_0 = 0.1$, and $\gamma = 0.1$ ($k_B T/\Gamma = 1$). The other parameters as in Fig.1.

both thermopower and figure of merit are larger in the antiparallel configuration, whereas the thermal conductance is larger in the parallel configuration. The difference between S (and also ZT) in the parallel and antiparallel configurations is clearly visible at the corresponding peaks, where it can be quite significant. In turn, the difference between heat conductances in both configurations is rather small and well resolved only in the vicinity of the relevant resonances. Anyway, Fig.7 reveals the possibility of constructing a *heat spin valve*, which would be a heat analog of the usual current spin valve. The suppression of thermal conductance in the antiparallel magnetic configuration is of similar origin as the suppression of linear electric conductance. The latter was accounted for by Julliere in terms of the two current model⁶⁵, and is due to different densities of states at the Fermi level in both configurations for electrons of a given spin orientation. More specifically, in the parallel configuration there is one spin channel (corresponding to

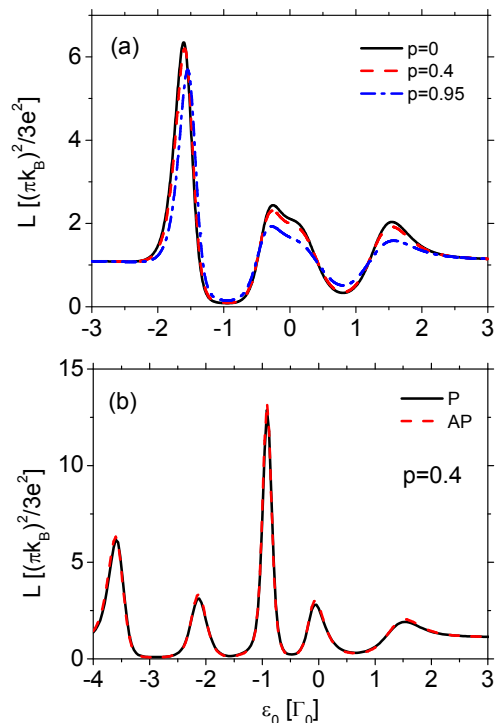


FIG. 9: (color online) Lorentz ratio as a function of the dots' levels energy calculated for indicated values of the leads' polarization p . Part (a) corresponds to parallel configuration and $U = 0$, while part (b) to $U/\Gamma_0 = 2$ and for parallel (P) and antiparallel (AP) magnetic configurations. The other parameter as in Fig.8.

high density of states in the source and drain electrodes) with high electric (and also heat) conductance and one with low conductance (corresponding to low density of states in the source and drain electrodes). In turn, in the antiparallel configuration both conduction channels have reduced conductance as now each of them corresponds to high density of states in one electrode and low density of states in the second electrode.

Now let us discuss briefly the temperature regime $k_B T/\Gamma_0 \approx \gamma$ ($k_B T/\Gamma \approx 1$). In Fig. 8 the thermoelectric coefficients are displayed for indicated values of the leads' polarization, no Coulomb interaction, and for parallel magnetic configuration. One can notice, that the thermal conductance increases with increasing leads' polarization p . In turn, the magnitudes of the thermopower as well as of the figure of merit decrease with increasing p . Similar behavior has been also reported for a single quantum dot attached to ferromagnetic leads.²¹

Although the quantum interference effects become *smearred out* by increasing temperature, the largest changes in the thermopower for $k_B T/\Gamma_0 \approx 1$ still occur in the vicinity of the antibonding level, where the conductance is strongly suppressed for $k_B T/\Gamma \ll 1$. Therefore, the figure of merit ZT achieves there relatively high values (above 30 in Fig.8(c)). All this leads to violation of the Wiedemann-Franz law, which can be measured by the

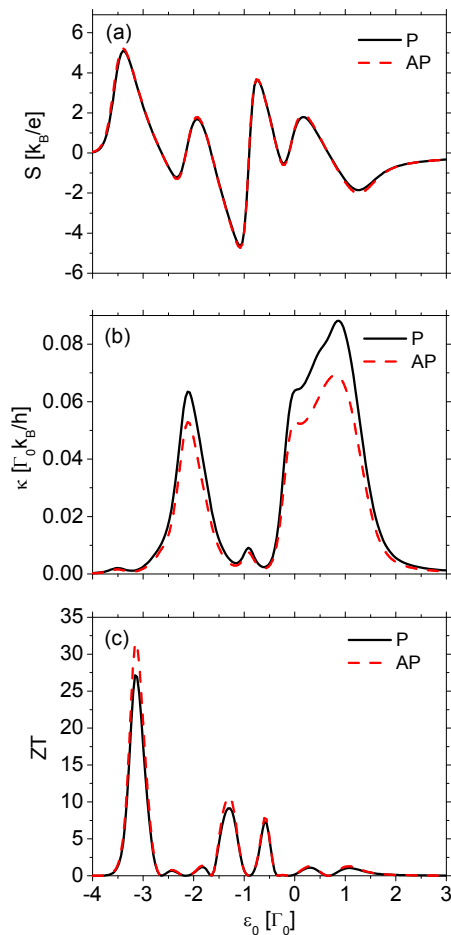


FIG. 10: (color online) Thermoelectric coefficients: (a) thermopower, (b) thermal conductance, (c) the figure of merit, as a function of the position of the dots' energy levels calculated for parallel (P) and for antiparallel (AP) magnetic configurations, and for $p = 0.4$. The other parameters as in Fig.8.

Lorenz ratio, $L = \kappa/GT$, as shown explicitly in Fig. 9, where the Lorenz ratio is displayed for indicated values of the leads polarization p and for interacting ($U \neq 0$) and non-interacting ($U = 0$) cases. One can note that the Coulomb interactions lead to larger deviations from the Wiedemann-Franz law, especially in the vicinity of the symmetry point $\varepsilon_0 = -U/2$ [Fig. 9(b)].

Similarly as for the temperature range studied before, thermoelectric coefficients depend on magnetic configuration, too. By changing magnetic configuration of the system from parallel to antiparallel one, the thermoelectric efficiency increases and is comparable to that obtained for $p = 0$. This is because in the antiparallel magnetic configuration both electric and thermal conductance decrease (see Fig. 10(b) for the thermal conductance). However, the latter suffers a larger drop and thus the figure of merit increases.

B. Spin bias and spin thermoelectric effects

Assume now that spin accumulation in the external leads becomes relevant, which may happen when spin relaxation time in the leads is sufficiently long. In such a case we have to take into account spin splitting of the electro-chemical level in both leads. Accordingly, the bias is then spin dependent and the difference in chemical potentials, $\Delta\mu_\sigma$, in the spin channel σ can be written as (see section 2 for details); $\Delta\mu_\sigma \equiv eV_\sigma = e(V + \delta V^s)$. Of course, the spin bias V^s vanishes in the absence of spin accumulation.

As we have already mentioned in the introduction, thermally induced spin voltage has been observed recently in ferromagnetic metallic slabs.⁵⁵ A consequence of this is a spin analog of the Seebeck effect, so-called spin Seebeck effect (or spin thermopower). In the following we present some numerical results for the spin thermoelectric effects in the system under consideration, especially for the spin thermopower and spin analog of the figure of merit. The latter quantity is defined as $Z^s T = (2e/h)G^s S^s T/\kappa$

In Fig. 11 we present the spin thermoelectric coefficients in the case of $k_B T/\Gamma = 1$. Since the basic features of the thermopower S are similar to those obtained and discussed earlier, we focus only on the spin thermopower S^s , see Fig.11(a). The spin thermopower depends on the leads' polarization more strongly than the thermopower S . Note, S^s vanishes in the limit of $p = 0$ and $|S^s|$ grows up with increasing p . Comparing Fig. 11 and Fig. 8 one finds that the sign of the spin thermopower S^s is opposite to the sign of the charge thermopower S . This is because the voltage drop induced in the spin minority channel is larger than that induced in the spin majority channel. Generally, the spin thermopower vanishes at the same level positions as the charge thermopower does. Similar behavior refers to the spin conductance shown in Fig. 11(b). It vanishes for $p = 0$ and grows with increasing p , being positive in Fig.11(b). The spin analog of the figure of merit, $Z^s T$, is shown in Fig. 11(c). It obviously grows up with increasing p as a result of the increase of both $|S^s|$ and G^s and a rather weak dependence of the thermal conductance on the leads polarization. The corresponding figure of merit ZT is shown in Fig. 11(d). ZT calculated on the condition of vanishing currents in both spin channels depends on the magnetic polarization of the leads in a more complex way than ZT obtained on the condition of $J = 0$. Roughly speaking, it grows up (drops) with increasing p for $\varepsilon_0 > 0$ ($\varepsilon_0 < 0$). The suppression of ZT corresponds to the regions where the thermopower S is almost independent of the spin polarization of the leads.

Qualitatively similar behavior of the spin thermoelectric coefficients can be observed also in the low temperature regime, $k_B T/\Gamma \ll 1$, as shown in Fig. 12 for a relatively high polarization factor, $p = 0.9$. The maximum value of spin figure of merit $Z^s T$ is now slightly higher than that in Fig.11, contrary to ZT which now is signif-

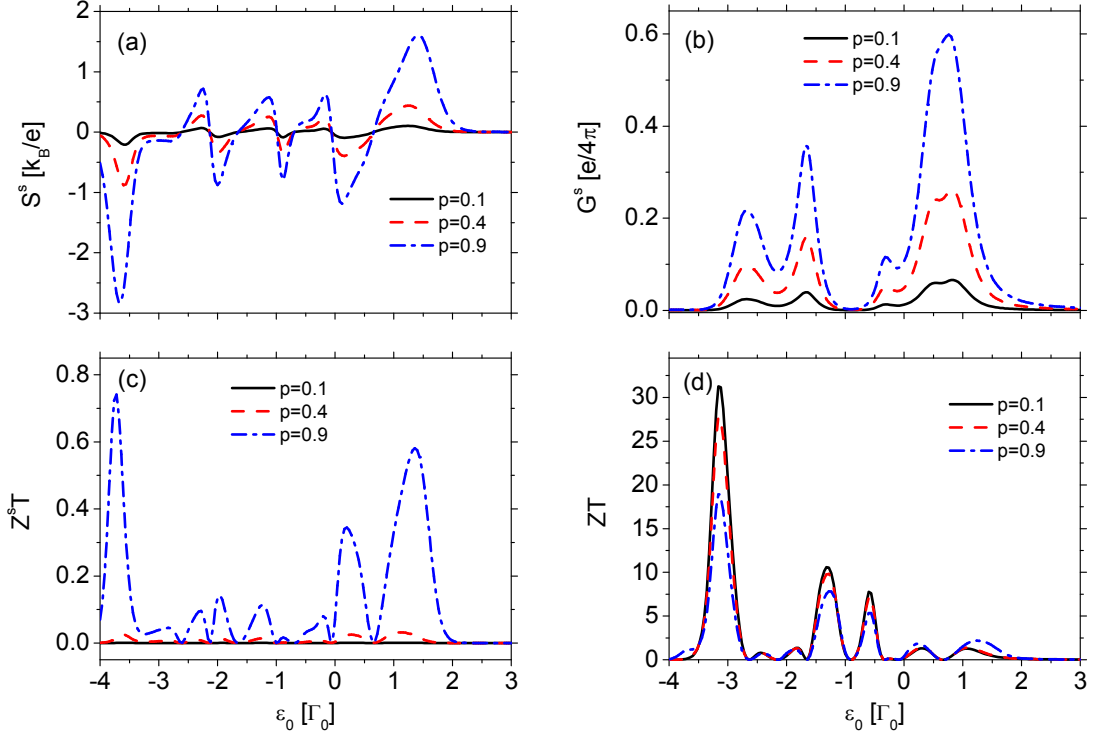


FIG. 11: Spin thermoelectric coefficients: (a) spin thermopower, (b) spin conductance, (c) $Z^s T$, (d) ZT , calculated as a function of the dots' levels energy for indicated values of the leads polarization p in the parallel magnetic configuration. The other parameters: $k_B T/\Gamma_0 = 0.1$, $\gamma = 0.1$, $t/\Gamma_0 = 0.8$, $\alpha = 0.15$, $U/\Gamma_0 = 2$, $q = 1$.

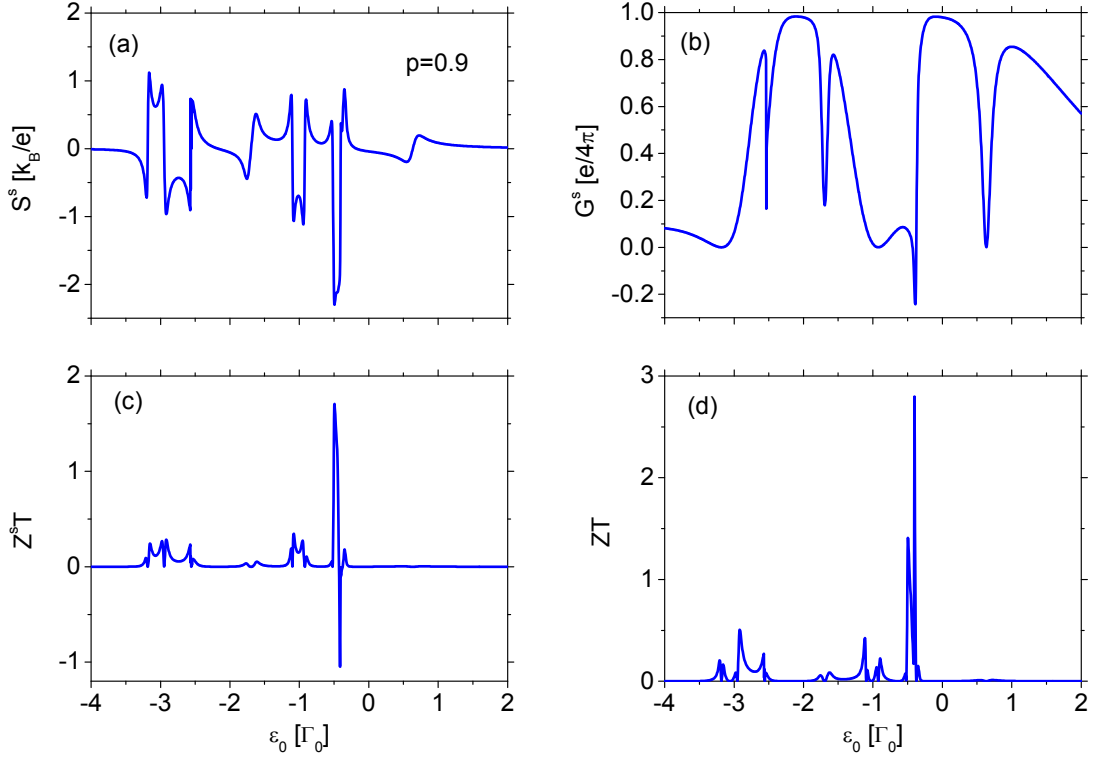


FIG. 12: Spin thermoelectric coefficients: (a) spin thermopower, (b) spin conductance, (c) $Z^s T$, (d) ZT , calculated as a function of the position of the dot levels for indicated values of the leads polarization p in the parallel magnetic configuration. The other parameters: $k_B T/\Gamma_0 = 0.01$, $\gamma = 1$. The other parameters as in Fig.11.

icantly smaller than in the case shown in Fig.11. Apart from this, one feature deserves mentioning here, i.e. the appearance of a negative spin conductance, which appears in some regions of the dots' energy levels. This, in turn, leads to negative values of the spin figure of merit Z^sT , see Fig. 12(c). Moreover, the spin conductance is now enhanced in comparison to that shown in Fig.11(b).

IV. SUMMARY

We have analyzed thermoelectric effects, like thermopower, electronic contribution to heat conductance, and thermoelectric efficiency in a system of two coupled quantum dots. The key point of the analysis was the role of interference effects (especially of the Fano antiresonances). We have shown that the interference effects can significantly enhance the thermoelectric efficiency, especially for specific thermal energy ranges. The thermoelectric efficiency can be additionally enhanced by Coulomb interactions. Thus, the thermoelectric efficiency can be controlled by temperature, Coulomb interactions and quantum interference effects. Moreover, we have also shown that the thermoelectric efficiency can be additionally controlled by asymmetry of the coupling of a given electrode to the two dots. Some of the parameters, especially coupling between the two dots and between the dots and leads can be tuned by external gate voltages. It is more difficult to control Coulomb parameter U , although it can be also tuned by changing size of the dots via additional gates.

We have also considered spin thermoelectric phenomena, in particular the spin analog of the thermopower – the so-called spin thermopower or spin Seebeck effect. The latter effect occurs as a result of spin asymmetry of the two spin channels. From the experimental point of view, the spin thermopower may be observed when the spin relaxation time in the external leads is sufficiently long, so the spin accumulation may build up. We have also analyzed the corresponding spin figure of merit.

As we have already mentioned above, the interference effects (like Fano resonance) can significantly enhance the thermoelectric efficiency of a device. The results presented include only electronic contribution to the heat current. However, one should bear in mind that there is also an additional phonon term in the heat conductiv-

ity, and this contribution to heat transport may reduce the thermoelectric efficiency presented above, especially at higher temperatures.^{42,66} At low temperatures, however, this contribution is small and therefore the results reported in this paper present a reasonable and satisfactory description. The formula for thermoelectric figure of merit, including the phonon contribution, can be written as $ZT = ZT_e/(1 + \kappa_{ph}/\kappa_e)$, where κ_{ph} is the phonon contribution to the heat conductance and ZT_e is the figure of merit of pure electronic origin (obtained assuming $\kappa_{ph} = 0$). Since the high thermoelectric efficiency corresponds to a significant suppression of the electronic thermal conductance near the antibonding state, it is evident that the phonon contribution to the thermal conductance, especially at high temperatures, may play a significant role and can not be neglected. However, it has been shown recently that the phonon thermal conductance may be remarkably reduced in properly prepared silicon nanowire nanojunctions^{15,17,67}, leading to impressive values of ZT ($ZT > 1$) at room temperature. The phonon contribution to the heat conductance in quantum dot systems can also be significantly suppressed by appropriate design of the device⁶⁸ (by creating a vacuum layer). Following Ref. 68, we have estimated the magnitude of ZT at $k_B T = 10\Gamma$ assuming experimentally available values of Γ , $\Gamma \approx 2.5$ meV (which is experimentally available in semiconducting quantum dots). Accordingly, for $T \approx 300K$ we find the maximum value of ZT to be of an order of $ZT \approx 18$. To reduce the phonon contribution to heat conductance one can also design the system using phononic crystals as the elements of leads⁶⁹. Furthermore, one can also minimize the probability of phonon transmission utilizing strong phonon reflection at the interfaces constructed from materials of dissimilar vibrational spectra.⁷⁰ In turn, calculating the phonon contribution to the heat conductance according to Ref. 71, one finds ZT up to 8, even in the absence of a vacuum layer.

Acknowledgments

This work was supported by Polish Ministry of Science and Higher Education partly as a research project in years 2010 – 2013 and partly as a research project in years 2009-2011.

* Electronic address: ptrocha@amu.edu.pl

† Electronic address: barnas@amu.edu.pl

¹ R. Franz, G. Wiedemann, Ann. Phys. (Berlin) **165**, 497 (1853).

² M. Cutler and N. F. Mott, Phys. Rev. **181**, 1336 (1969).

³ L. D. Hicks and M. S. Dresselhaus, Phys. Rev. B **47**, 16631 (1993).

⁴ C. W. J. Beenakker and A. A. M. Staring, Phys. Rev. B **46**, 9667 (1992).

⁵ Y. M. Blanter, C. Bruder, R. Fazio, and H. Schoeller, Phys. Rev. B **55**, 4069 (1997).

⁶ M. Turek and K. A. Matveev, Phys. Rev. B **65**, 115332 (2002).

⁷ J. Koch, F. von Oppen, Y. Oreg, and E. Sela, Phys. Rev. B **70**, 195107 (2004).

⁸ B. Kubala and J. König, Phys. Rev. B **73**, 195316 (2006).

⁹ X. Zianni, Phys. Rev. B **75**, 045344 (2007).

¹⁰ X.-M. Zhang, X. Chen, W. Lu, Phys. Lett. A **372**, 2816

- (2008).
- ¹¹ B. Kubala, J. König, and J. Pekola, *Phys. Rev. Lett.* **100**, 066801 (2008).
 - ¹² P. Murphy, S. Mukerjee, and J. Moore, *Phys. Rev. B* **78**, 161406(R) (2008).
 - ¹³ R. Venkatasubramanian, *Recent Trends in Thermoelectric Materials Research III, Semiconductors and Semimetals Vol. 71* (Academic Press, New York, 2001), pp. 175201; G. Chen, *Recent Trends in Thermoelectric Materials Research III, Semiconductors and Semimetals Vol. 71* (Academic, New York, 2001), pp. 203259.
 - ¹⁴ P. Reddy, S. Y. Jang, R. A. Segalman, and A. Majumdar, *Science* **315**, 1568 (2007).
 - ¹⁵ A. I. Hochbaum, R. Chen, R. D. Delgado, W. Liang, E. C. Garnett, M. Najarian, A. Majumdar, and P. Yang, *Nature (London)* **451**, 163 (2008).
 - ¹⁶ K. Baheti, J. A. Malen, P. Doak, P. Reddy, S. Y. Jang, T. D. Tilley, A. Majumdar, and R. A. Segalman, *Nano Lett.* **8**, 715 (2008).
 - ¹⁷ A. I. Boukai, Y. Bunimovich, J. Tahir-Kheli, J. K. Yu, W. A. Goddard III, and J. R. Heath, *Nature (London)* **451**, 168 (2008).
 - ¹⁸ K. Schwab, E. A. Henriksen, J. M. Worlock, and M. L. Roukes, *Nature (London)* **404**, 974 (2000).
 - ¹⁹ L. G. C. Rego and G. Kirczenow, *Phys. Rev. Lett.* **81**, 232 (1998).
 - ²⁰ Y. Dubi and M. Di Ventra, *Nano Lett.* **9**, 97 (2009).
 - ²¹ R. Świrkowicz, M. Wierzbicki, and J. Barnaś, *Phys. Rev. B* **80**, 195409 (2009).
 - ²² T. Markussen, A. P. Jauho, and M. Brandbyge, *Phys. Rev. B* **79**, 035415 (2009).
 - ²³ M. Galperin, A. Nitzan, and M. A. Ratner, *Mol. Phys.* **106**, 397 (2008).
 - ²⁴ A. M. Lunde, K. Flensberg, and L. I. Glazman, *Phys. Rev. Lett.* **97**, 256802 (2006).
 - ²⁵ D. Segal, *Phys. Rev. B* **72**, 165426 (2005).
 - ²⁶ F. Pauly, J. K. Viljas, and J. C. Cuevas, *Phys. Rev. B* **78**, 035315 (2008).
 - ²⁷ Y.-S. Liu, Y. -R. Chen, and Y. -C. Chen, *ACS Nano* **3**, 3497 (2009).
 - ²⁸ J. P. Bergfield, M. A. Solis, and C. A. Stafford, *ACS Nano* **4**, 5314 (2010).
 - ²⁹ D. Boese and R. Fazio, *Europhys. Lett.* **56**, 576 (2001).
 - ³⁰ B. Dong and X. L. Lei, *J. Phys.: Condens. Matter* **14**, 11747 (2002).
 - ³¹ M. Krawiec and K. I. Wysokinski, *Phys. Rev. B* **73**, 075307 (2006).
 - ³² R. Sakano, T. Kita, and N. Kawakami, *J. Phys. Soc. Jpn.* **76**, 074709 (2007).
 - ³³ T.-S. Kim and S. Hershfield, *Phys. Rev. B* **67**, 165313 (2003).
 - ³⁴ R. Scheibner, H. Buhmann, D. Reuter, M. N. Kiselev, and L. W. Molenkamp, *Phys. Rev. Lett.* **95**, 176602 (2005).
 - ³⁵ R. Franco, J. Silva-Valencia, M.S. Figueira, *J. Magn. Magn. Mater.* **320**, 242 (2008).
 - ³⁶ M. Yoshida and L. N. Oliveira, *Physica B* **404**, 3312 (2009).
 - ³⁷ T. A. Costi and V. Zlatić, *Phys. Rev. B* **81**, 235127 (2010).
 - ³⁸ M. Wierzbicki and R. Świrkowicz, *J. Phys.: Condens. Matter* **22**, 185302 (2010).
 - ³⁹ J. Liu, Q.-F. Sun, and X. C. Xie, *Phys. Rev. B* **81**, 245323 (2010).
 - ⁴⁰ D. M.-T. Kuo, *Jpn. J. Appl. Phys.* **48**, 125005 (2009).
 - ⁴¹ M. Hatami, G. E. W. Bauer, Q. Zhang, and P. J. Kelly, *Phys. Rev. B* **79**, 174426 (2009).
 - ⁴² G. J. Snyder and E. S. Toberer, *Nature* **7**, 105 (2008).
 - ⁴³ J.-S. Wang, J. Wang, and J. T. Lü, *Eur. Phys. J. B* **62**, 381 (2008).
 - ⁴⁴ Y. Dubi and M. Di Ventra, *Rev. Mod. Phys.* **83**, 131 (2011).
 - ⁴⁵ Z.-Y. Zhang, *J. Phys.: Condens. Matter* **19**, 086214 (2007).
 - ⁴⁶ F. Chi, J. Zheng, X. -D. Lu, K. -C. Zhang, *Phys. Lett. A* **375**, 1352 (2011).
 - ⁴⁷ M. Wierzbicki and R. Świrkowicz, *Phys. Rev. B* **84**, 075410 (2011).
 - ⁴⁸ G. Gómez-Silva, O. Ávalos-Ovando, M. L. Ladrón de Guevara, and P. A. Orellana, e-print arXiv:1108.4460v2.
 - ⁴⁹ P. Trocha, J. Barnaś, *Phys. Rev. B* **76**, 165432 (2007).
 - ⁵⁰ P. Trocha and J. Barnaś, *J. Nanosci. Nanotechnol.* **10**, 2489 (2010).
 - ⁵¹ D. Loss and E. V. Sukhorukov, *Phys. Rev. Lett.* **84**, 1035 (2000).
 - ⁵² M. L. Ladrón de Guevara, F. Claro, P. A. Orellana, *Phys. Rev. B* **67**, 195335 (2003).
 - ⁵³ Y. -S. Liu and X. F. Yang, *J. Appl. Phys.* **108**, 023710 (2010).
 - ⁵⁴ O. Karlström, H. Linke, G. Karlström, A. Wacker, *Phys. Rev. B* **84**, 113415 (2011).
 - ⁵⁵ K. Uchida, S. Takahashi, K. Harii, J. Ieda, W. Koshibae, K. Ando, S. Maekawa, and E. Saitoh, *Nature (London)* **455**, 778 (2008); K. Uchida, T. Ota, K. Harii, S. Takahashi, S. Maekawa, Y. Fujikawa, E. Saitoh, *Solid State Commun.* **150**, 524 (2010).
 - ⁵⁶ M. Johnson, R.H. Silsbee, *Phys. Rev. B* **35**, 4959 (1987).
 - ⁵⁷ J. Shi, K. Pettit, E. Kita, S.S.P. Parkin, R. Nakatani, M.B. Salamon, *Phys. Rev. B* **54**, 15273 (1996).
 - ⁵⁸ L. Gravier, S. Serrano-Guisan, F. Reuse, and J.-P. Ansermet, *Phys. Rev. B* **73** 024419 (2006).
 - ⁵⁹ L. Gravier, S. Serrano-Guisan, F. Reuse, and J.-P. Ansermet, *Phys. Rev. B* **73** 052410 (2006).
 - ⁶⁰ Y. Dubi and M. Di Ventra, *Phys. Rev. B* **79**, 081302(R) (2009).
 - ⁶¹ Y. -S. Liu, F. Chi, X. -F. Yang, and J. -F. Feng, *J. Appl. Phys.* **109** 053712 (2011).
 - ⁶² T. Rejec, R. Žitko, J. Mravlje, and A. Ramšak, e-print arXiv:1109.3066v1.
 - ⁶³ J. M. Ziman, *Electrons and Phonons. The Theory of Transport Phenomena in Solids* (Oxford University Press, 1960).
 - ⁶⁴ W. G. van der Wiel, S. D. Franceschi, J. M. Elgerman, S. Tarucha, and L. P. Kouwenhoven, *Rev. Mod. Phys.* **75**, 1 (2002).
 - ⁶⁵ M. Julliere, *Phys. Lett. A* **54**, 225 (1975).
 - ⁶⁶ N. Stojanovic, D. H. S. Maithripala, J. M. Berg, and M. Holtz, *Phys. Rev. B* **82**, 075418 (2010).
 - ⁶⁷ T. Markussen, A. P. Jauho, and M. Brandbyge, *Phys. Rev. Lett.* **103**, 055502 (2009).
 - ⁶⁸ David M.-T. Kuo and Y.-C. Chang, *Phys. Rev. B* **81**, 205321 (2010).
 - ⁶⁹ A. N. Cleland, D. R. Schmidt, and C. S. Yung, *Phys. Rev. B* **64**, 172301 (2001).
 - ⁷⁰ W. Kim, R. Wang, and A. Majumdar, *Nano Today* **2**, 40 (2007).
 - ⁷¹ M. Tsaousidou and G. P. Triberis, *J. Phys.: Condens. Matter* **22**, 355304 (2010).